Dependence of Electrical Breakdown on Spherulite Size in Isotactic Polypropylene

B. V. CERES and J. M. SCHULTZ, *Department of Chemical Engineering, University of Delaware, Newark, Delaware 19711*

Synopsis

A self-seeding technique, coupled with isothermal crystallization, was used to prepare isotactic polypropylene specimens of varying spherulite size, but of constant crystallinity and lamellar thickness. The latter quantities were also varied by changing the isothermal crystallization temperature. The electrical lifetime at constant applied voltage, in a point-plane geometry, was measured. It was found that the electrical lifetime decreased with increasing spherulite size and, more weakly, with decreasing crystallinity (at a given spherulite size).

INTRODUCTION

Electrical breakdown of insulation is a major problem in the communication and power transmission industries. The breakdown sites within the polymeric insulator are localized as "trees." The trees form gradually, before the ultimate breakdown, as narrow channels running outward from the conductor of a high voltage cable. The existence of relationships between electrical treeing and the microstructure of the insulation could prove instrumental in tailoring high quality electrical insulation. In this case, the pertinent microstructural features would include the spherulite size, lamellar thickness, and degree of crystallinity. These features can be controlled almost independently, thus providing a range of morphologies.

There have been several previous studies of morphology in the initiation and growth of trees.[1-7] It has been shown by Wagner[1] that electrical trees in polypropylene follow spherulitic boundaries. It has been demonstrated that a linear relation between the treeing inception voltage[6] and the spherulite radius exists. It has recently been suggested that the breakdown originates from amorphous zones.[7] However, in all existing correlations of macroscopic breakdown strength and microstructure, the microstructural features have never been controlled such that only one feature is varied, while the others remain constant. For instance, variations in solidification conditions usually cause simultaneous variation in spherulite size, lamellar thickness, and degree of crystallinity, and it is not possible in such cases to uniquely establish property–microstructure correlations. The emphasis in the present work, on the other hand, is in specimen preparation, isolating spherulite size variation from other microstructural changes. To this end, a technique of self-seeded isothermal crystallization is used.

The microstructure of semicrystalline polymers is dependent on the thermal history. At the spherulite level, the final spherulite diameter is dictated primarily by the volumetric nucleation rate. Were the material free from heterogeneities which could act as nucleation sites, then the volumetric

Journal of Applied Polymer Science, Vol. 29, 4183–4197 (1984)
 CCC 0021-8995/84/124183-15$04.00

nucleation rate $\dot{N}$ (nuclei per unit volume per unit time) would be dictated by thermal fluctuations and the sporadic formation of crystal nuclei. This ideal almost never obtains; spherulite nuclei almost always form at specific heterogeneities, either at remnants of former crystals or at foreign surfaces. Elevating the temperature of a polymeric mass over its equilibrium melting point does not immediately destroy all traces of crystallinity. Rather, local crystal memory disappears gradually, at a degree and rate which increases with temperature. If one heats an already crystallized specimen to temperatures T_1 above the equilibrium melting point T^0_m, one should find fewer and fewer nuclei remaining as T_1 increases. One may then quench from various T_1 to a given isothermal crystallization temperature $T_2 < T^0_m$. In this case, the higher the temperature T_1, the larger the mean spherulite diameter.[8–12] On the other hand, the lamellar thickness is independent of the temperature T_1.[13] The use of specific melt temperatures to control the density of residual nuclei is termed "self-seeding."

The crystallization temperature itself offers an important control of spherulite size. Since nucleation rate, be it homogeneous or heterogeneous, increases with degree of undercooling below the melting point, the final spherulite size decreases with increasing undercooling (or, by extension, with cooling rate). This is probably the most extensively used means of controlling spherulite size,[14–20] but has the disadvantage that other microstructural detail also varies with undercooling, especially at the crystallite size level. It has been demonstrated numerous times,[16,21–32] by both x-ray small angle scattering and by transmission electron microscopy, that the crystallite thickness increases with increasing crystallization temperature. Further, the overall mass fraction of the material which is in the crystalline state at room temperature also increases with crystallization temperature,[21,25,29,33,34] and with time of crystallization[33] or of annealing.[29]

In the present work, self-seeding, coupled with isothermal crystallization, is used to control the spherulite size, independently of other microstructural features. Lamellar thickness and degree of crystallinity are controlled by varying the temperature of crystallization.

EXPERIMENTAL

Specimen Preparation

A Hercules Profax isotactic polypropylene molding compound was used. Data on the specific material is not available.

In order to produce specimens with varying spherulite size, but constant lamellar spacings and crystallinities, a three-step, self-seeding process was used. The thermal history of one specimen is shown in Figure 1. All specimens are given the same initial melting and crystallization treatment (step I). Specifically, the specimen, in the form of a 3.18 mm thick plate, is held at 240°C, and 1500 psi for 45 min and then cooled in air to room temperature. The specimen is then taken from room temperature to a temperature T_1 above the melting point T_m and held there for a prescribed period of time (45 min). This is step II. During step II, the overall crystallinity is destroyed, but some density of easy crystal nucleation sites remains. The higher the

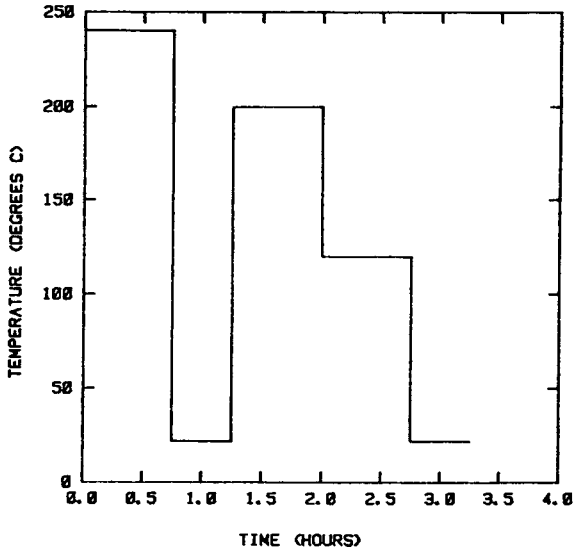

Fig. 1. Time–temperature plot for a polypropylene specimen melt-treated at 200°C and then crystallized at 120°C.

temperature T_1, the smaller the number of residual nuclei. In the present work, the temperature T_1 ranged from 195 to 225°C. Specimens were held at a pressure of 1500 psi during step II. In step III, each specimen is quenched into an oil bath, fixed at a given temperature T_2, below the melting point and allowed to crystallize there (under atmospheric pressure) for 45 min. Following this crystallization treatment, the specimen is allowed to cool in air to room temperature. The temperatures T_2 used here were 120, 130, 140, and 150°C.

Specimens crystallized at a given temperature T_2 from a set of temperatures T_1 should have varying spherulite sizes at constant other microstructure. Specimens with constant spherulite size, but varying lamellar spacing or crystallinity could be found among material crystallized at various temperatures T_2.

Microstructure Characterization

Spherulite Size. For the examination of spherulite size, thin sections were obtained, using a Sorvall MTl Ultramicrotome. Sectioning was done at room temperature, using a glass knife. A typical section appears as shown in Figure 2. From 100× photographs, the diameters of a random selection of 10 spherulites with distinct boundaries (those whose diameters lie near the plane of the section) were measured. The arithmetic mean of those diameters was used to denote the spherulite diameter.

Figure 3 shows average spherulite diameters versus melt temperature T_1. As expected, the spherulite size increases with increasing T_1.

Density and Small-Angle X-Ray Scattering (SAXS). A density gradient column, filled with a hexane–carbon tetrachloride mixture held at room temperature, was used. Specimen densities were read after 6 h in the column.

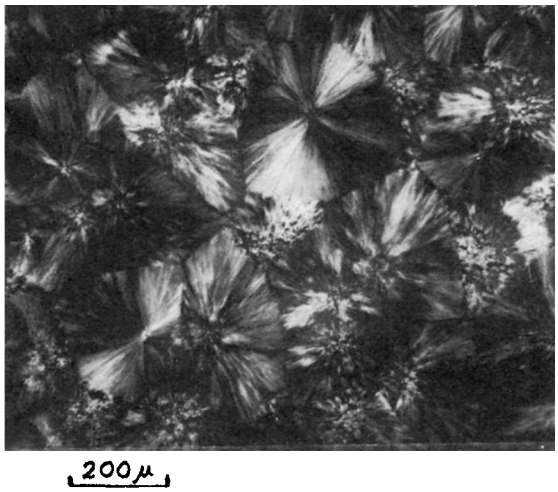

Fig. 2. Photomicrograph of a thin section from material melt-treated at 225°C and crystallized at 130°C.

SAXS was used to quantify the lamellar spacing. Measurements were made using the ORNL 10-Meter SAXS Instrument.[35] This instrument utilizes a rotating anode x-ray source, (CuK) graphite crystal monochromatization, pinhole collimation, and a 2-dimensional position-sensitive detector. All data were radially averaged. A typical scan appears in Figure 4. Lamellar spacings are derived from the position of the hump, using Bragg's law.

Density and SAXS data were used to determine the lamellar thickness d from the lamellar spacing and the mass fraction crystallinity c, according to $d = \phi_c l$.

Figure 5 shows lamellar thickness and overall density vs. the crystallization temperature T_2. Within relatively narrow scatter bands, these quan-

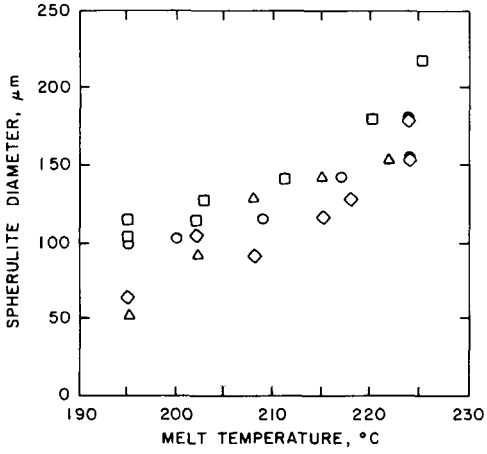

Fig. 3. Spherulite diameter versus melt temperature. Crystallization temperatures (°C): (△) 120; (□) 130; (◇) 140; (○) 150.

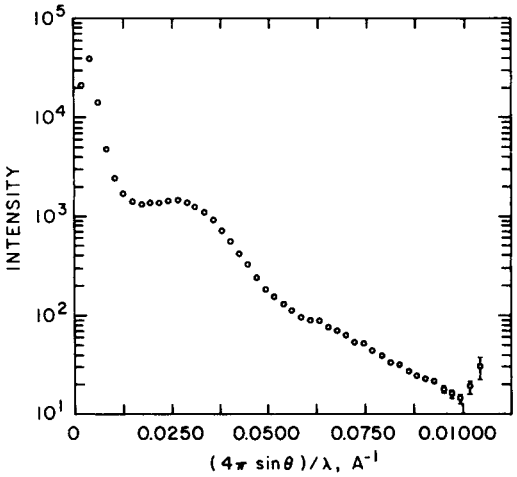

Fig. 4. Intensity vs. $(4\pi \sin \theta)/\lambda$ for material melt-treated at 195°C and crystallized at 120°C.

tities are constant for a given crystallization temperature. It should be pointed out that one expects that d and ϕ_c should monotonically increase with T_2. This was not observed here. The reason is that 45 min was not sufficient at 140 and 150°C to complete the primary crystallization of the material. Thus for those temperatures, crystallization took place largely during the cooling treatment.

Crystallinity and lamellar thickness correlate well, as shown in Figure 6.

Electrical Breakdown

The electrical breakdown system employs a single needle/ground plate geometry, as sketched in Figure 7. The needle electrode is a 1-mm steel rod with a 30° cone tip. The radius of the tip is 3 mm. The needle electrode is held in place by a small hole found at the end of a Lucite arm. The ground plate is a 12.5 cm square copper sheet mounted on four ceramic standoffs. The needle/ground plate assembly is completely contained in a Lucite box

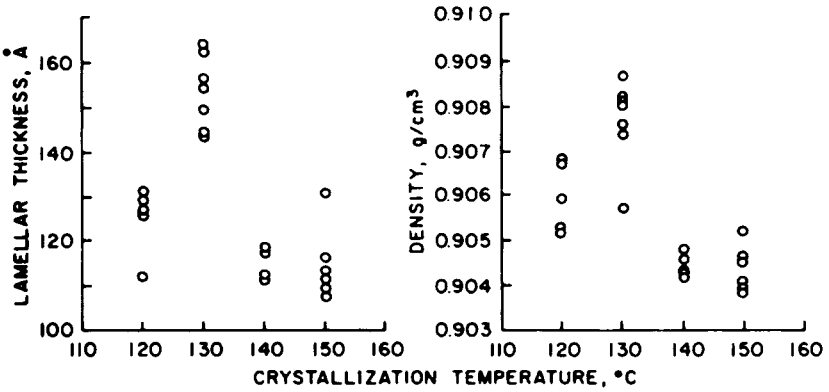

Fig. 5. Lamellar thickness and density versus crystallization temperature.

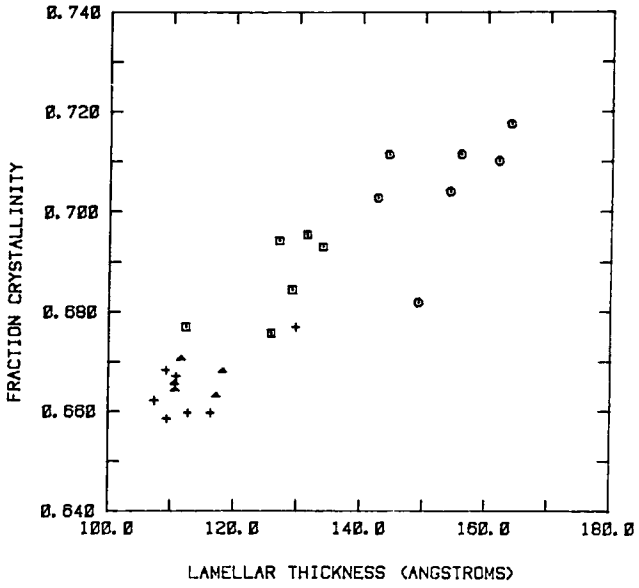

Fig. 6. Degree of crystallinity vs. lamellar thickness. Crystallization temperatures (°C): (⊡) 120; (⊙) 130; (▲) 140; (+) 150.

and surrounded by a dielectric grade silicone oil (Dow-Corning 200) with a viscosity of 50 cS.

All results reported in the next section relate to the propagation of breakdown of specimens in which breakdown has already been initiated. The initiation of breakdown begins with the creation of a small indentation in the samples' surface from the sharp tip of the needle electrode. A needle injection device is utilized to measure the depth of the indentation with the aid of a micrometer. The electrode is injected into the sample with two complete turns of the micrometer knob to a depth of 0.13 cm. The electrode is left in the indentation for 30 s.

The electrode is then retracted and repositioned over the indentation, flush to the surface of the specimen. In air, a voltage of 11.9 kV is then applied, at a rate of 1 kV/s. The specimen is left at this voltage for 5 min. During this period, due to the air environment, ionization erodes the base of the indentation. This is the initiation step. The power is then cut, and

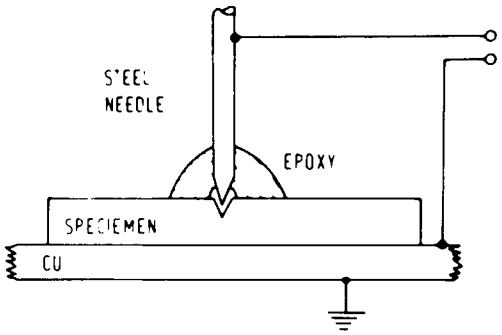

Fig. 7. Schematic of electrical breakdown specimen and electrode geometry.

the electrode positioned to the same depth as previously recorded. At this point the sample is ready for propagation.

In order to establish a controlled vented propagation test, the electrode must be sealed to the sample. With the electrode in place, an epoxy cement (Hysol EA 9309) was made to surround the electrode-specimen interface. All specimens were tested immediately after the 24-h curing time of the epoxy.

For each specimen the time to breakdown was measured. An apparatus was designed to allow time measurement and power shutdown at breakdown. At breakdown, a surge of current passes through the specimen and is grounded through the earth ground. At this point, a small winding on the ground side generates a voltage which is detected by a breakdown circuit. The circuit relays a small line current to a solid state relay, and then the power and a timer are turned off. The entire event takes place in less than a millisecond. This allows minimum damage to the sample during breakdown and measures the electrical breakdown time. A schematic of the circuit is given in Figure 8.

The study of electrical treeing followed immediately. The specimen was placed back in the specimen box (which was now half-filled with oil). It was necessary to insure that the specimen had a good seal on the ground plate. The gate was closed, and again the variac was set at zero. The power supply was turned on and the voltage was raised to 11.5 kV at a rate of 1 kV/s. The clock time was recorded and recorded again when the sample failed. The elapsed time was the breakdown time, and the parameter was used as the determinant of the sample's insulating strength.

All samples were tested following the same procedure. Furthermore, it was decided that the samples would be initiated consecutively so that one

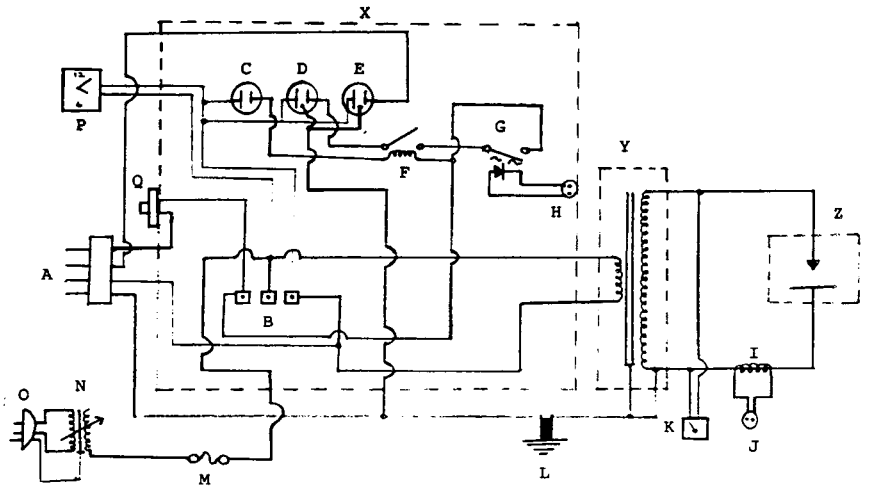

Fig. 8. Schematic of electrical breakdown test circuit: (A) 208V plug; (B) terminals; (C) door interlock receptacle; (D) strip power receptacle; (E) sensor power receptacle; (F) door relay; (G) solid state switch; (H) line input to breakdown sensor; (I) pulse solenoid pickup; (J) line output to breakdown sensor; (L) ground plate; (M) 3 A fuse; (N) Variac; (O) plug to strip power; (P) timer; (Q) 5 A fuse; (X) control box enclosure; (Y) transformer enclosure; (Z) specimen box.

would not need to empty the specimen box many times. In order to eliminate any effects of the epoxy drying, once the 24-h drying period had ended, the specimens were immediately propagated. Once the sample had failed, the electrode was replaced for the next sample. During breakdown, due to the current surge, the tip of the electrode was damaged and could not be used again.

RESULTS

Figure 9 shows the air-channel created by the initiation treatment. The V-shaped portion at the top is created by the mechanical injection of the cone-tip electrode. The spike emanating from the cone is a breakdown channel (an electrical treeing "trunk"). The length of a typical initiation channel is 0.15 cm. The purpose of the initiation channel is similar to that of a sharp notch in fracture mechanics investigations; that is, the failure nucleation event is circumvented. Since failure nucleation (both electrical and mechanical) is very sensitive to accidental surface flaws, it is very useful to remove nucleation from consideration. It is important, however, to keep in mind that only the growth stage of the breakdown channel (the tree) is measured here; it is not known what portion of the total electrical life (i.e., nucleation plus growth) this represents.

Figure 10 shows a typical tree formed during breakdown. All trees were found to be branchlike—i.e., a major breakdown channel with branches emanating from that channel. This form is in agreement with the observations of Noto and Yashimura,[36] done under similar test conditions. In Figure 10, the actual breakdown channel is much larger than the adjacent branch. The lateral expansion of the main channel most probably occurred under the current surge at breakdown.

It is important also to establish that the breakdown measured here is really of the controlled vented type. That is, simple air ionization of a specimen (uncontrolled venting) does not result in a treeing type breakdown,

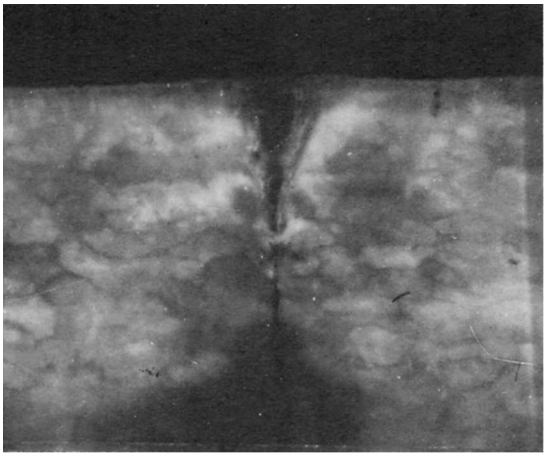

Fig. 9. Micrograph of the channel produced during initiation.

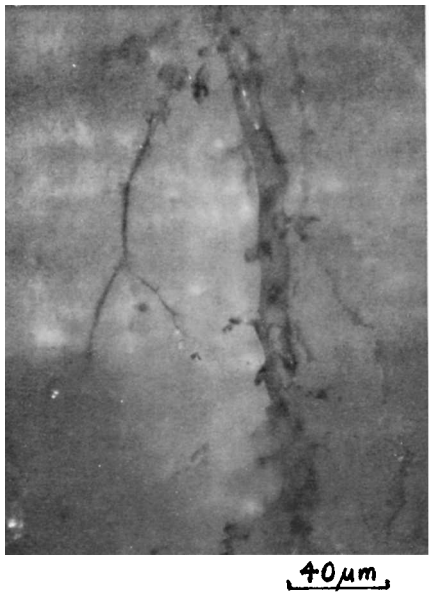

Fig. 10. Micrograph of developed electrical tree.

whereas breakdown under a limited supply of air (controlled breakdown) does. In the present work, one specimen was indented and air ionized (no epoxy electrode encapsulation and no silicone oil environment) until breakdown. The breakdown time in this case was 45 min, about 1/5 the average breakdown time of the other specimens. Only one main breakdown channel was seen.

In the present case, the breakdown channels followed the spherulite boundaries. Figure 11 shows a thin section normal to the mean field di-

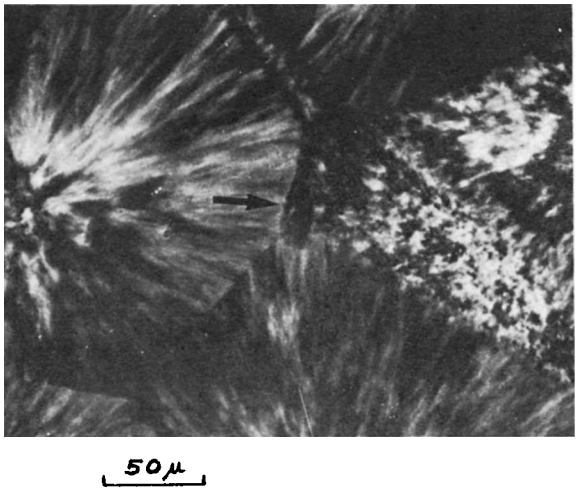

Fig. 11. Thin section perpendicular to the field axis. The arrow points to hollow discharge channel at spherulite boundary.

rection. In the center of the micrograph a channel forming a hole at a spherulite boundary can be seen.

Figure 12 shows the correlation between breakdown time t_b and spherulite diameter for the four crystallization bath temperatures T_1 used. Except for the 120°C data, which are inconclusive, all data show a trend of decreasing t_b with increasing T_1. The data for T_1 = 140°C and T_1 = 150°C fall in the same band, as expected, since in both cases crystallization occurred during cooldown to room temperature. Figure 13 shows least-squares linear fitting to the 130°C and 140°C data. Both data sets are fit by an equation of the form

$$t_B = a - bD$$

where D is the spherulite diameter. The slope b is identical for the two cases.

Figures 14 and 15 show the correlation between t_B and the other microstructural characteristics, lamellar thickness and crystallinity. No correlation between breakdown time and these characteristics can be seen.

DISCUSSION

It has been demonstrated above that spherulite boundaries have a major impact on the electrical life of polypropylene. Two anciliary questions are addressed in this section. Those questions are: "Why are spherulite boundaries effective as tree channels?" and "Is there really no evidence for an electrical breakdown role for microstructure at other levels?"

That spherulite boundaries act as preferred paths for electrical treeing must relate to some sort of singularity at the boundaries. In fact, spherulite boundaries can offer singularities in at least three ways. They are sites of elastic discontinuity,[37] often resulting in fracture along the boundaries.[38-42] They can be compositionally different from the intraspherulitic material, since noncrystallizable or poorly crystallizable material is pushed ahead of the growing spherulitic front and collects at the spherulite bound-

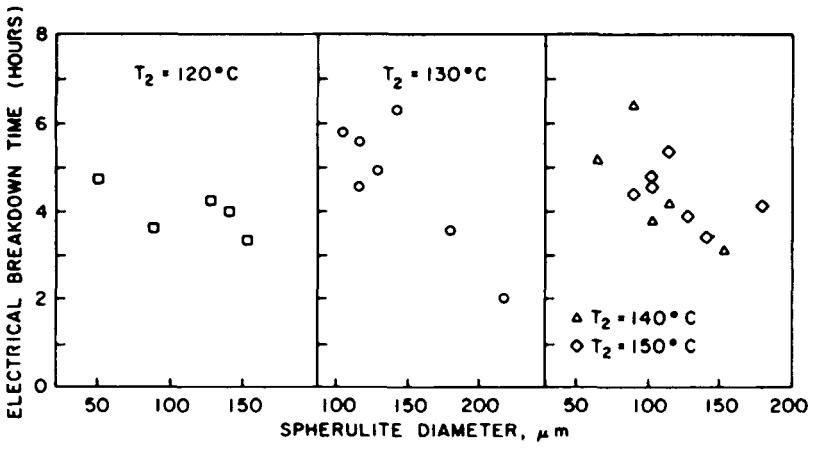

Fig. 12. Electrical breakdown time vs. spherulite diameter for different crystallization bath temperatures T_2.

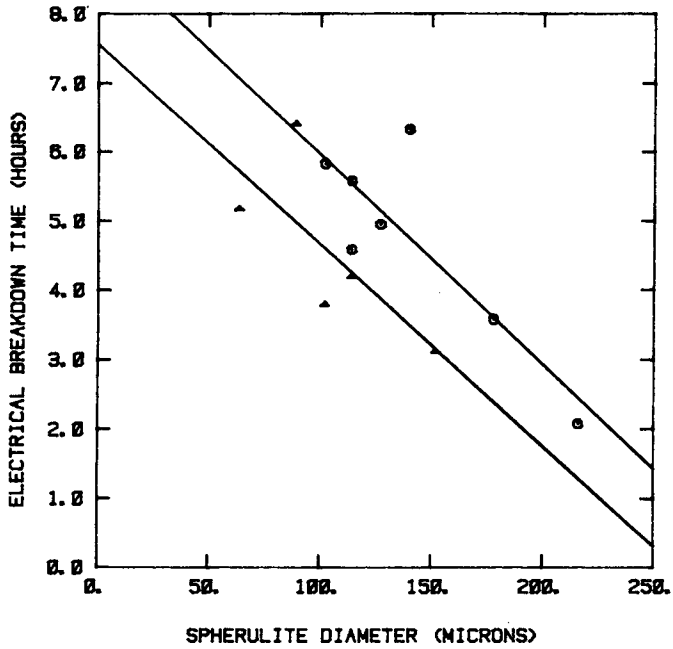

Fig. 13. Least square lines through data for $T_2 = 130°C$ and $T_2 = 140°C$.

aries.[43-46] Finally, since the solidified material is more dense than the melt from which it grows, there is a density deficiency which must accumulate at the last enclaves to solidify—the nodes at which three or more neighboring spherulites grow together. The size, size distribution, and spacial distribution of such interspherulitic voids has been analyzed by Galeski and

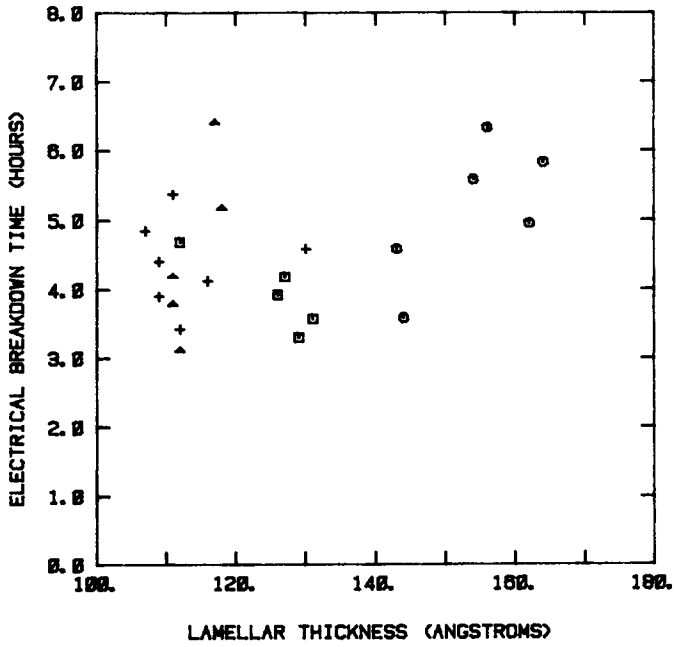

Fig. 14. Electrical breakdown time versus lamellar thickness: Crystallization temperatures (°C): (□) 120; (⊙) 130; (▲) 140; (+) 150.

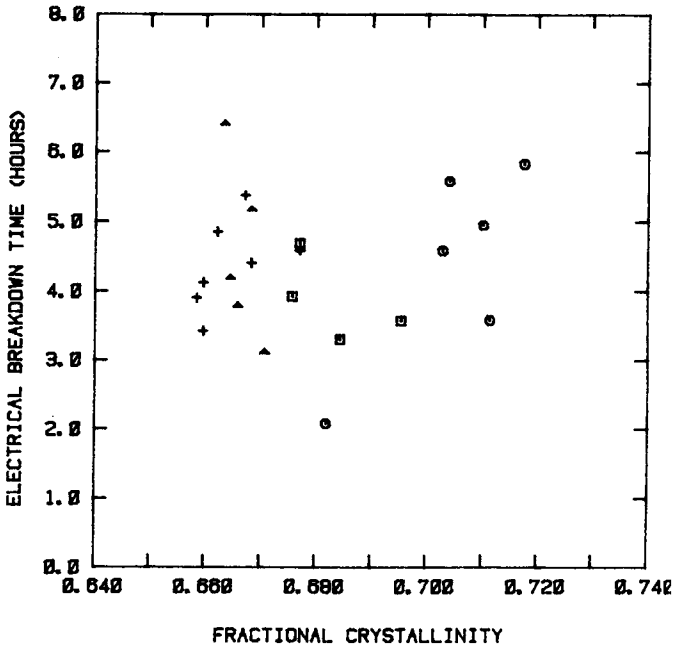

Fig. 15. Electrical breakdown time versus degree of crystallinity: Crystallization temperatures (°C): (□) 120; (⊙) 130; (▲) 140; (+) 150.

Piorkowska[47,48] and observed directly by Way et al.[38] and Muccigresso and Phillips.[49] All three types of singularity are accentuated as the spherulite size increases. Hence any of these could act as the underlying source of spherulite boundary electrical weakness.

The results of the present investigation could provide evidence for one or another of the mechanisms. Consider the effect of crystallization rate. The more rapid the spherulite growth rate, the less selective is the spherulite with regard to poorly crystallizable molecules. Consequently, the boundary composition problem should decrease with increasing spherulite growth rate. The data of Figure 13 show, however, that the faster-crystallizing material (the 140°C data) shows a generally lower electrical life than the slower growing (130°C) material. A comparison of 120 and 130°C data leads to the same conclusion, since the growth rate at 120°C is higher than at 130°C. Thus the material which should have the greatest foreign atom concentration at the boundary shows the highest electrical life. Similarly, the mechanical fragility of the spherulite boundary increases with increasing overall crystallinity,[37] again indicating that the 130°C boundaries should be the most prone to mechanical failure. Thus it seems likely that neither mechanical fragility nor foreign molecules contribute significantly in the present case.

It appears that voiding may also not be critical. Recall that voiding occurs because of a specific volume difference between spherulite and melt. Thus the total interspherulitic volume of voiding should increase with increasing crystallinity (i.e., increasing spherulite density). This is not observed. Figure 15 showed no global trend of electrical life with crystallinity. In fact, if electrical lifetime is plotted against crystallization temperature for a given

spherulite size range, a trend to longest electrical lifes at a crystallization temperature of 130°C is seen. This is shown in Figure 16. This is inverse to the trend which would be expected, were boundary voiding to be controlling.

From the above, it is to be concluded that the singularities considered—noncrystallizable layer, mechanical vulnerability, and voiding—are either unimportant or are only weakly dependent on crystallization conditions.

Figure 16 indicates that crystallinity or lamellar thickness plays a role. The form of the crystallization temperature dependence of electrical lifetime seen in Figure 16 is similar to the dependences of crystallinity and of lamellar thickness (Fig. 5). Thus it appears that, at a given spherulite size, the electrical life increases with the degree of crystallinity. This is consistent with the general behavior of polymer insulators, in that it has been known for some time that electrical strength increases generally with the level of crystallinity (see Ref. 50 for a review). It is possible that this trend relates to the resistance of the material at the tip of a tree channel to channel propagation by mechanical or erosive action of the gas within the channel. In this sense, one would view the spherulite boundaries as always the globally weakest sites in the material, but with an absolute sensitivity to attack which increases with the overall level of crystallinity of the material.

SUMMARY

It has been demonstrated that the electrical lifetime of isotactic polypropylene decreases with increasing spherulite size. A weaker trend of electrical lifetime to increase with crystallinity, at constant spherulite size

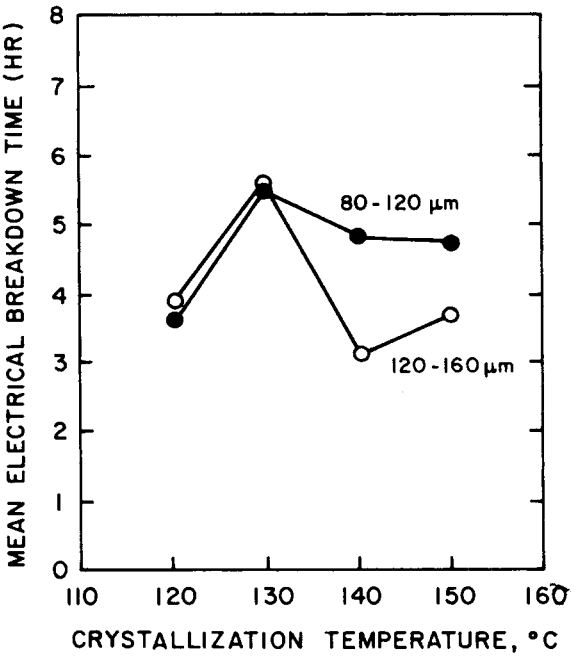

Fig. 16. Mean electrical breakdown time versus crystallization temperature, for two different spherulite size ranges.

has also been noted. No clear definition of the underlying source of spherulite boundary weakness has emerged.

We are especially grateful to the Delaware Power and Light Company for the gift of high voltage ac transformers, to Mr. Herbert Wardell of the Institute of Energy Conversion of the University of Delaware, whose advise on high voltage technology was very useful, to Dr. E. McMahon of E. I. DuPont de Nemours, Inc., whose expertise helped guide the early stages of this work, to Mr. Joseph Dombrowski, who designed and built the breakdown circuitry, to Dr. J. S. Lin, who allowed use of the ORNL 10-Meter SAXS Instrument and who assisted in the SAXS data collection and analysis, and to Professor Roger Wagner, who generously permitted us to use his microtomy facilities.

References

1. H. Wagner, *Ann. Rep. Conf. Elec. Insul. Dielectr. Phenom. (CEIDP)*, 62 (1975).
2. P. J. Phillips, *IEEE Trans.*, **EI-13**, 451 (1978).
3. J. Muccigrasso and P. J. Phillips, *IEEE Trans.*, **EI-13**, 172 (1978).
4. D. V. Brower, K. L. Naylor and P. J. Phillips, *CEIDP*, 113 (1980).
5. S. R. Barnes, *Polymer*, **21**, 723 (1980).
6. S. M. Kolesov, *IEEE Trans.*, **EI-15**, 382 (1980).
7. T. Fukuda, S. Irie, Y. Asada, M. Maeda, H. Nakagawa, and N. Yamada, *IEEE Trans.*, **EI-17**, 386 (1982).
8. F. Khoury, *J. Polymer Sci.*, **26**, 375 (1957).
9. A. Sharples, *Polymer*, **3**, 250 (1962).
10. J. H. Magill, *J. Appl. Phys.*, **35**, 3249 (1964).
11. V. A. Kargin, T. I. Sogolova, and L. I. Nadaieishvili, *Polymer Sci. USSR*, **6**, 1404 (1964).
12. J. H. Reinshagen and R. W. Dunlap, *J. Appl. Polymer Sci.*, **17**, 3619 (1975).
13. D. C. Bassett, *Principles of Polymer Morphology*, Cambridge University Press, Cambridge, 1981.
14. F. J. Padden, Jr. and H. D. Keith, *J. Appl. Phys.*, **30**, 1479 (1959).
15. Y. F. Yu and R. Ullman, *J. Polymer Sci.*, **60**, 55 (1962).
16. F. Rybnikář, *Coll. Czech., Chem. Commun.*, **31**, 4080 (1966).
17. J. Patel and P. J. Phillips, *J. Polym. Sci., Polym. Lett. Ed.*, **11**, 771 (1973).
18. J. D. Hoffman, L. J. Frolen, G. S. Ross, and J. I. Lauritzen, Jr., *J. Res. Natl. Bur. Stand., Sect. A*, **79**, 671 (1975).
19. J. Maxfield and L. Mandelkern, *Macromolecules*, **10**, 1141 (1977).
20. K. Friedrich, *Prog. Colloid Polym. Sci.*, **64**, 103 (1978).
21. L. Mandelkern, A. S. Posner, A. F. Diorio, and D. E. Roberts, *J. Appl. Phys.*, **32**, 1509 (1961).
22. J. J. Weeks, *J. Res. Natl. Bur. Stand., Sect. A.*, **67**, 441 (1963).
23. P. H. Geil, *Polymer Single Crystals*, Wiley-Interscience, New York, 1963.
24. J. D. Hoffman and J. J. Weeks, *J. Chem. Phys.*, **42**, 4301 (1965).
25. L. Mandelkern, J. M. Price, M. Gopalan, and J. G. Fatou, *J. Polymer Sci.*, **4A-2**, 385 (1966).
26. D. R. Carter and E. Baer, *J. Appl. Phys.*, **37**, 4060 (1966).
27. F. Rybnikář, *Coll. Czech., Chem. Commun.*, **32**, 1913 (1967).
28. J. J. B. P. Blais and R. St. John Manley, *J. Macromol. Sci. Phys.*, **B1**, 525 (1967).
29. S. Kavesh and J. M. Schultz, *J. Polym. Sci.*, **9A-2**, 85 (1971).
30. P. J. Barham, R. A. Chivers, D. A. Jarvis, J. Martinez-Salazar, and A. Keller, *J. Polym. Sci., Polym. Lett. Ed.*, **19**, 539 (1981).
31. R. A. Chivers, P. J. Barham, J. Martinez-Salazar, and A. Keller, *J. Polym. Sci., Polym. Phys. Ed.*, **20**, 1717 (1982).
32. P. J. Barham, D. A. Jarvis, and A. Keller, *J. Polym. Sci., Polym. Phys. Ed.*, **20**, 1733 (1982).
33. M. J. McCready, J. M. Schultz, J. S. Lin, and R. W. Hendricks, *J. Polym. Sci., Polym. Phys. Ed.*, **17**, 725 (1979).
34. L. Mandelkern, M. Glotin, and R. A. Benson, *Macromolecules*, **14**, 22 (1981).
35. R. W. Hendricks, *J. Appl. Cryst.*, **11**, 15 (1978).

36. F. Noto and N. Yoshimura, *1974 Ann. Rep. Conf. Elect. Insul. Dielectr. Phenom.*, 207 (1975).
37. J. M. Schultz, *Polym. Eng. Sci.*, **24**, 770 (1984).
38. J. L. Way, J. R. Atkinson, and J. Nutting, *J. Mater. Sci.*, **9**, 293 (1974).
39. K. Friedrich, *Prog. Colloid Polym. Sci.*, **64**, 103 (1978).
40. E. Hornbogen and K. Friedrich, *J. Mater. Sci.*, **15**, 2175 (1980).
41. K. Friedrich and U. A. Karsch, *J. Mater. Sci.*, **16**, 2167 (1981).
42. A. Sandt, Doktorarbeit, Ruhr-Universitat Bochum, 1981.
43. J. L. Way and J. R. Atkinson, *J. Mater. Sci.*, **6**, 102 (1971).
44. J. Dlugosz, G. V. Fraser, D. Grubb, A. Keller, J. A. Odell, and P. L. Gogin, *Polymer*, **17**, 471 (1976).
45. P. D. Calvert and T. G. Ryan, *Polymer*, **19**, 611 (1978).
46. S. W. Rowe and R. Tobazeon, *J. Mater. Sci.*, **16**, 2608 (1981).
47. A. Galeski and E. Piorkowska, *J. Polym. Sci., Polym. Phys. Ed.*, **21**, 1299 (1983).
48. A. Galeski and E. Piorkowska, *J. Polym. Sci., Polym. Phys. Ed.*, **21**, 1313 (1983).
49. J. Muccigresso and P. J. Phillips, *IEEE Trans. El. Insul.*, **EI-13**, 172 (1978).
50. R. Fava, in *Treatise on Materials Science, Vol. 10B, Properties of Solid Polymeric Materials*, J. M. Schultz, Ed., Academic, New York 1977.

Received October 3, 1983
Accepted April 2, 1984